

This is the peer reviewed version of the following article:

On the identification of the angular position of gears for the diagnostics of planetary gearboxes / D'Elia, G; Mucchi, E.; Cocconcelli, Marco. - In: MECHANICAL SYSTEMS AND SIGNAL PROCESSING. - ISSN 0888-3270. - 83:(2017), pp. 305-320. [10.1016/j.ymssp.2016.06.016]

*Terms of use:*

The terms and conditions for the reuse of this version of the manuscript are specified in the publishing policy. For all terms of use and more information see the publisher's website.

20/05/2025 11:23

(Article begins on next page)

1 On the identification of the angular position of gears for  
2 the diagnostics of planetary gearboxes

3 G. D'Elia<sup>a</sup>, E. Mucchi<sup>a</sup>, M. Cocconcelli<sup>b</sup>

4 <sup>a</sup>*Engineering Department in Ferrara - Università degli Studi di Ferrara Via Saragat, 1 -*  
5 *44122 Ferrara, Italy*

6 <sup>b</sup>*Department of Science and Engineering Methods - University of Modena and Reggio*  
7 *Emilia Via G. Amendola, 2 - Pad. Morselli - 42123 Reggio Emilia, Italy*

---

8 **Abstract**

Generally, in planetary gearbox diagnostics, vibration transducers are placed on the gearbox case near the ring gear. The relative angular position of the planet gears with respect to the transducer is a **useful information** for the evaluation of vibration signals related to planet/sun gears. This angular position is usually unknown, or it is known with a large tolerance causing serious difficulties in both gears and bearing diagnostics. In fact, noise and spurious component from healthy planets could overhang the informative content about incipient faults. The present work seeks to propose two alternative methods for the precise identification of the angular position of the planet gears with respect to the transducer. The first one is based on the study of how the power flows inside the Time Synchronous Average of the ring gear, whilst the second method is based on a modified statistical parameter such as the Crest Factor. The effectiveness of these methods is assessed on the basis of actual vibration signals acquired from a faulty planetary gearbox. The knowledge of the exact angular position of the planet gears allows the diagnostics of both gears and bearings, as proven by extensive experimental activities reported in the paper.

9 *Keywords:*

10 planetary gearbox, diagnostics, vibrations, time synchronous average

---

*Email address: gianluca.delia@unife.it (G. D'Elia )*

## 11 1. Introduction

12 Bearings and gears are probably the most common components in ro-  
13 tating machines. Since they are functional for the dynamics of the rotating  
14 parts, [an incipient fault could lead to a sudden break of the machine](#). Thus,  
15 [possible](#) consequences are safety problems, irreparable damage of the ma-  
16 chine, and high costs of non-production that normally exceed the cost of  
17 the machine. Consequently, the diagnostics of these components has always  
18 played a great interest in both academy and industry. The study of failure  
19 detection in bearings started over two decades ago, embracing a crowd of  
20 signal processing techniques which deals with several domains, from time to  
21 time-frequency. An emerging interest has been reported on modelling rotat-  
22 ing machine signals as cyclostationary [1], which embodies a particular class  
23 in the realm of non-stationary stochastic processes [2]. From the pioneering  
24 work of McCormick and Nandi [3] the principles of cyclostationarity have  
25 become the state-of-art in bearing diagnostics [4]. Above all, Antoni in [5]  
26 discusses which cyclic spectral tool is the most suitable for the localised fault  
27 detection in ball bearings. In particular the operator that describes how  
28 the power flows within the signal was introduced by Antoni a few years ago  
29 [6]. Diagnostics becomes more complex when bearings and gears are coupled  
30 together as in gearboxes. Among them the class of planetary gearboxes is  
31 probably the most challenging. The difficulty of extracting the bearing char-  
32 acteristic fault frequencies of a planetary gear bearing stems from two factors.  
33 First, transducers may only be placed on the exterior of the gearbox, usually  
34 rather far from bearings. Second, the rotational axes of the planet gears are  
35 not fixed, i.e. they move with respect to the gearbox housing and thus to the  
36 transducers. As a result, the vibration signature of the planet gear bearings  
37 can be altered by the variable transfer path. In this scenario, standard signal  
38 processing techniques fail, and the characteristic bearing fault frequencies  
39 cannot be extracted from the vibration signals. [For example envelope analy-  
40 sis, which is a widely used technique, could fail due to spurious components  
41 that overhang the fault signature. Indeed the working conditions of a specific  
42 gearbox could increase or reduce the fighting chance of the standard tech-  
43 nique](#). Time synchronous averaging (TSA) has been shown to be a useful tool  
44 for extracting gear mesh vibrations from composite vibration signals since it  
45 enables the extraction of periodic signals from noise-polluted signals [7, 8, 9].  
46 The resulting vibration signal corresponds to one complete revolution of the  
47 gear under consideration, and thus changes in the vibration waveform due

48 to damage on individual teeth can be identified. The application of the TSA  
49 for the extraction of periodic waveforms in ordinary gearbox was proposed  
50 by Braun in the mid 70s [7]. However, such TSA techniques relate to gears  
51 with fixed vibration transfer paths from the source of the vibration to the  
52 transducer. In planetary gearboxes, the vibration transfer path is not fixed  
53 but it is subjected to variation due to the relative motion of the planet gears  
54 with respect to the transducer.

55 A technique for the evaluation of the TSA vibration signals associated  
56 with the sun and planet gears of a planetary gearbox was proposed by P.D.  
57 McFadden in the early 90s [10]. Such a work demonstrates that, for planetary  
58 gearboxes with certain geometric properties, the averaged vibration signals  
59 can be extracted from a vibration signal captured by a single fixed-frame  
60 transducer. Subsequent studies validated the McFadden's research and pre-  
61 sented slight variations on the technique [11, 12]. Samuel and Pines [12]  
62 incorporates the use of multiple sensors in the evaluation of planet and sun  
63 gear TSAs. The use of multiple sensors overcome several limitations such  
64 as: i) capturing all the teeth of planet and sun gear in planetary gearboxes  
65 with non appropriate geometric properties, ii) reduce the time required for  
66 performing the planet and sun gear TSAs and iii) increasing the robustness  
67 of the extraction method in case of sensor failure. However, the fundamental  
68 methodology remains unchanged; moreover [12] does not focus the attention  
69 on the evaluation of the relative position between planet gears and trans-  
70 ducer.

71 The TSA of the planet/sun gears can be obtained if and only if, the  
72 relative position of the planet gears with respect to a transducer placed on  
73 the ring gear is known a priori. In [13] McFadden suggested that the position  
74 of each of the planet gears with respect to the transducer, could be estimated  
75 directly from the TSA of the ring gear by identifying the locations of the  
76 maximum vibration amplitude. This identification could be more effective  
77 from the amplitude modulated signal of the ring gear. For small planetary  
78 gearbox, this approach could be not effective and the planet position cannot  
79 be identified leading to a poor evaluation of the planet gear TSA, as outlined  
80 in the following.

81 This paper focuses on fixed ring gear epicyclic gear train working on the  
82 hypothesis of steady speed. In particular two alternative methods are pro-  
83 posed for the precise identification of the position of each of the planet gears  
84 with respect to the transducer. Once the vibration signal related to each  
85 gearbox components is determined, diagnostics of gears is straightforward

86 by means of any of the established methods proposed in the literature.  
87 Moreover, also the diagnostics of the gearbox bearings is now possible, since  
88 Cyclic Power technique works on a vibration signal which is free from compo-  
89 nents other than the one under study. The aim of this paper is to propose a  
90 methodology for the diagnostics of a planetary gearbox as a whole, including  
91 both gears and bearings.

92 The paper is organised as follows. After a brief introduction and problem  
93 statement given in this Section, the TSA algorithm proposed by McFadden  
94 is outlined in the next. The two proposed methods for the evaluation of  
95 the planet gear positions are presented in Section 3. The effectiveness of the  
96 proposed diagnostics methods is discussed on the basis of real data in Section  
97 4 for both gears and bearings. Section 5 addresses the concluding remarks.

## 98 2. Background on TSA in planetary gearbox

99 McFadden and Smith [14] have demonstrated that as a given planet gear  
100 approaches the transducer, the measured vibration level increases, while as  
101 the planet gear moves away from the transducer the measured vibration level  
102 decreases. Let us introduce  $h(t)$  the transfer function between the transducer  
103 and the planet gear, with a period of one carrier revolution  $T_c$ , Figure 1.  
104 Thus, planet signal  $x(t)$  as seen by transducer  $j$  is given by  $h_j(t)x(t)$ .

105 In order to extract the planet/sun signal McFadden stated that [14] :  
106 “when a given planet gear is near a transducer, the vibrations measured by  
107 the transducer are dominated by the meshing of that specific planet gear with  
108 the sun and ring gears.” Thus, during each passing of a given planet, a  
109 small data window can be collected. It can be assumed that over the width  
110 of such a window, the transfer function between the accelerometer and the  
111 region of tooth contact will remain constant. The planet gear teeth in mesh  
112 can be determined at each carrier revolution, and the window of data can  
113 be stored in a buffer according to the meshing tooth. This process is then  
114 repeated several times, in order to obtain a window of data for each tooth  
115 of the planet gear. The so arranged buffer includes the vibration signal for a  
116 complete revolution of the planet gear. Several buffers can then be averaged  
117 in order to obtain the TSA signal of the gear of interest, Figure 2.

118 Mathematically speaking, let us define a windowing function centered at  
119 time  $t = nT_c$ , where  $n$  is an integer number. The time at which  $h_j(t)$  reaches  
120 its maximum is defined by  $v(t - nT_c)$ , Figure 1 (c). The subsequent windowed  
121 vibration signal is given by expression  $h_j(t)x(t)v(t - nT_c)$ .

122 Let the window width be chosen as an integer number of tooth mesh  
 123 period  $T_m$ , given by [13]:

$$T_v = N_v T_m \quad (1)$$

124 If  $N_v$  is chosen to be appropriately small, the amplitude of  $h_j(t)$  can be  
 125 assumed to be constant ( $H_{j,0}$ ) over the entire window, and the vibration  
 126 signal becomes:

$$h_j(t)x(t)v(t - nT_c) = H_{j,0}x(t)v(t - nT_c) \quad (2)$$

127 Once a window of vibration data has been obtained, it must be mapped  
 128 into the appropriate location in a buffer for synthesizing the planet/sun gear  
 129 vibration signal. To determine this location a sampling function  $g(t) =$   
 130  $g(t - nT_g)$  can be used, where  $T_g$  is the rotation period of the gear of interest  
 131 (planet/sun). The convolution operator can be used, leading to  $[H_{j,0}x(t)v(t -$   
 132  $nT_c)] * g(t)$ , in order to map the windows into the appropriate location. If  
 133 the tooth number of the gear of interest is  $N_g$ , once  $N_g$  windows have been  
 134 mapped, all of the teeth of the gear under consideration will be captured.

135 In order to extract the TSA vibration signal from the measured one,  
 136 a large number ( $N_e$ ) of synthesized signals (buffers) must be captured and  
 137 averaged. The TSA of the gear of interest is given by:

$$x_g(t) = \frac{1}{N_e N_v} \sum_{n=0}^{N_e N_g - 1} [H_{j,0}x(t)v(t - nT_c)] * g(t) \quad (3)$$

138 Therefore, in order to compute the planet/sun gear TSA, the signal should  
 139 be firstly angular resampled according to the period of rotation of the gear  
 140 of interest ( $T_g$ ). In order to do that, the carrier rotation frequency must to  
 141 be known; the rotation period of the gear of interest could be obtained by  
 142 multiplying the carrier rotation period by the Willis gear ratio between ring  
 143 gear and the gear of interest.

144 The number of carrier rotations that occur before the gear of interest will  
 145 return to its initial state relative to the ring gear is given by:

$$n_{Reset,g} = \frac{lcm(N_g, N_r)}{N_r} \quad (4)$$

146 where  $lcm$  stands for least common multiple and  $N_r$  is the number of ring  
 147 gear teeth. Therefore, a given tooth of the gear of interest will be aligned

148 (in case of planter gear, alignment implies meshing) with a given tooth of  
 149 the ring gear for a given carrier rotation only once every  $n_{Reset,g}$ . For each  
 150 carrier rotation, the sequence of aligned teeth can be found using:

$$P_{n,g} = \text{mod}(nN_r, N_g) + 1 \quad (5)$$

151 where *mod* is the modulus after division and  $n$  is the number of carrier  
 152 rotations. The tooth aligned in the initial state,  $P_{0,g}$ , is defined as tooth 1.  
 153 It can be seen that  $P_{0,g} = P_{n_{Reset,g}}$ .

### 154 3. On the planet-transducer position

155 Function  $h(t)$  is directly related to the mass, damping and stiffness prop-  
 156 erties of the gearbox. In some cases the combination of these properties  
 157 leads function  $h(t)$  to be particularly flat. Thus, no amplitude modulation  
 158 effects can be visible in the ring gear TSA, also after the application of the  
 159 amplitude demodulation techniques, e.g. the Hilbert Transform demodula-  
 160 tion [15] or the McFadden’s separation method as well [13]. The planet gear  
 161 position relative to the transducer cannot be pointed out, leading to a poor  
 162 evaluation of the planet gear TSA. Hereafter two methods are proposed in  
 163 order to identify the angular position of the planet gears with respect to the  
 164 transducer. The first one is based on the mean instantaneous power of the  
 165 ring gear TSA, whilst the second one is based on a “modified” Crest Factor.

#### 166 3.1. Method A: Power flow

167 The relative position of each of the planet gears with respect to the trans-  
 168 ducer could be estimated by studying how the power flows in the vibration  
 169 signal. In particular, the planet position could be determined from the power  
 170 flow of the ring gear TSA. As a matter of fact, each time a planet passes under  
 171 the transducer, an increase of the power released within the signal occurs.

172 The operator that describes how the power flows within the signal was  
 173 introduced by J. Antoni a few years ago [6]. Let  $x(t)$  be a continuous time  
 174 signal, the mean instantaneous power is defined as:

$$P_x(t) = \sum_{\alpha \in \mathcal{A}} P_x^\alpha e^{j2\pi\alpha t} \quad (6)$$

175 where  $P_x^\alpha$  is the cyclic powers of the signal at cyclic frequencies  $\alpha$ , defined  
 176 as:

$$P_x^\alpha = \lim_{T \rightarrow \infty} \frac{1}{T} \int_T |x(t)|^2 e^{-j2\pi\alpha t} dt \quad (7)$$

177 Set  $\mathcal{A}$  in equation (6) embraces all the cyclic frequencies inside  $x(t)$ .

178 In order to obtain the position of the planet gears with respect to the  
 179 transducer, the cyclic power is filtered around the cyclic frequency corre-  
 180 sponding to the number of gear teeth, with a bandwidth large enough to en-  
 181 compass a number of sidebands corresponding to the number of the planetary  
 182 gearbox planets. In particular, the whole procedure could be summarised as  
 183 follows:

184 - Evaluation of the ring gear TSA

185 - Evaluation of  $P_x^\alpha$  relative to the ring gear TSA (i.e. estimation of the  
 186 Fourier Transform of the squared absolute value of the ring gear TSA)

187 - Inclusion in set  $\mathcal{A}$  of the cyclic order equal to the number of the ring gear  
 188 teeth, as well as the left and right modulating sidebands corresponding  
 189 to the number of planet gears (i.e. filter the  $P_x^\alpha$  by taking into account  
 190 only the cyclic order equal to the number of ring gear teeth as well as  
 191 both the left and right sideband relative to the number of planet gears)

192 - Reconstruction of  $P_x$  based on set  $\mathcal{A}$  (i.e. estimation of the inverse Fourier  
 193 Transform of the filtered  $P_x^\alpha$ )

194 - Evaluation of the envelope of  $P_x$

195 - Every maxima in  $P_x$  envelope will give the time instant corresponding to a  
 196 constant phase value of successive planet with respect to the transducer  
 197 location.

198 Once one planet gear phase is evaluated, the phases of the other planet  
 199 gears can be obtained by taking into account the angle between two consecu-  
 200 tive planet gears by kinematics relations, or by taking into account the other  
 201 maxima.

### 202 3.2. Method B: Statistical Parameter

203 The position of a particular planet gear with respect to the transducer  
 204 can also be determined by the analysis of a simple statistical parameter. A



205 counterpart of the function  $P_x$  can be obtained by a tooth-wide evaluation  
 206 of a “Moving Crest Factor” (MCF). The MCF is defined as:

207

$$MCF = \frac{x(\tau)_{peak-peak}}{RMS(x(\tau))} \quad (8)$$

208

209 where  $x_{peak-peak}(\tau)$  is the peak to peak value and  $RMS(x(\tau))$  indicates  
 210 the RMS value. Time parameter  $\tau$  is used to stress the moving windowed  
 211 nature of the signal:  $x(\tau) = w(t - \tau_w)x(t)$ , where  $w$  is the windowing func-  
 212 tion and  $\tau_w$  the delay used according to the following procedure. Generally  
 213 speaking, the Crest Factor is a measure of how extreme the peaks are in a  
 214 waveform compared to the mean value. The peak to peak value is used in  
 215 equation (8) in order to increase the sensitivity of the genuine Crest Factor.  
 216 The MCF evaluated by equation (8) is not a function of time, but a single  
 217 numerical value. In order to obtain a function which could be related to  
 218 the signal power flow, Eq. (8) is evaluated on a signal portion embracing a  
 219 single ring gear tooth. Finally, the tooth-wide MCF is filtered around the  
 220 order of the planet carrier rotation which corresponds to the planet gear  
 221 number. De facto, the evaluation of MCF over a one tooth wide window,  
 222 set its sample frequency equals to the number of ring gear teeth. Because  
 223 the frequency range of interest is related to the number of planet gears, the  
 224 sample frequency of MCF is always greater enough to perfectly reconstruct  
 225 the waveform of interest. The maximum value of the so processed MCF gives  
 226 the position of one planet gear with respect to the transducer. The whole  
 227 procedure could be summarised as follows:

- 228 - Evaluation of the ring gear TSA
- 229 - Evaluation of the MCF for each ring tooth
- 230 - Filtering the tooth-wide MCF function around the order of the planet  
 231 carrier rotation which corresponds to the planet gear number
- 232 - Every maxima in the filtered tooth-wide MCF function will give the time  
 233 instant corresponding to a constant phase value of the successive planet  
 234 with respect to the transducer location.

235 As previously stated, once one planet gear phase is evaluated, the phases  
 236 of the other planet gears can be obtained by taking into account the angle  
 237 between two consecutive planet gears, or by taking into account the other

238 maxima. Moreover, phase distortion should be avoided during the filtering  
 239 operation. In this work an ideal FIR filter is used, which does not affect the  
 240 phase of the filtered signal.

Table 1: Induction motor data

	BN80C2	BN132MB4
Nominal power [ $kW$ ]	1.5	9.2
Nominal torque [ $Nm$ ]	5.1	61
Nominal speed [ $rpm$ ]	2800	1440
Number of poles per phase winding	2	4

#### 241 4. Experimental data analysis and discussion

242 This section aims at testing the effectiveness of the proposed methods for  
 243 both the diagnostics of gears and bearings on the basis of experimental data.  
 244 Tests were performed in a test-rig designed and built up at the Engineering  
 245 Department of the University of Ferrara. The test-rig consists of a base,  
 246 including two induction motors controlled by inverters and a planetary gear  
 247 unit (Figure 3). In more detail, the driving induction motor (BN80C2) is  
 248 controlled in a feedback speed loop; its speed is evaluated by an encoder  
 249 with 360 pulses per revolution. The load induction motor (BN132MB4) is  
 250 controlled in a feedback torque loop [by measuring the current absorbed in](#)  
 251 [the working condition](#), while the speed is evaluated by an encoder with 3600  
 252 pulses per revolution. Table 1 lists the data of the induction motors.

253 The tests were performed on a two-stage planetary gearbox. In particular,  
 254 the gear unit (MP 105 IS 2) is a two-stage on which each stage contains a  
 255 sun gear (27 teeth), three planets (39 teeth) and a ring gear (108 teeth) for  
 256 a global speed reduction ratio of 25. Table 2 lists the data of each gearbox  
 257 stage, [while Table 3 lists the aligned tooth of the gear planet with a given](#)  
 258 [tooth of the ring gear under the transducer, from 0 to 12 carrier rotations](#)  
 259 [\(Equation 5\). De facto, after 13 carrier rotations the planet gear return](#)  
 260 [to its initial state under the transducer \(Equation 4\). It is possible to see](#)  
 261 [from Table 3, that the minimum width of the window function allowing for](#)  
 262 [a complete reconstruction of the planet signal is 3 teeth. As stated in \[13\],](#)  
 263 [in order to reduce the error component in the planet signals, the windowed](#)  
 264 [signal extracted for each carrier rotation should overlap, therefore a window](#)

Table 2: Gear data

	First stage	Second stage
Sun gear teeth	27	36
Planet gear teeth	39	39
Ring gear teeth	108	108
Number of planets	3	3
Speed reduction ratio	5	4

Table 3: Sequence of planet gear teeth under the transducer for each carrier revolution, Equation 5

carrier rotation $n$	0	1	2	3	4	5	6	7	8	9	10	11	12
tooth #	1	31	22	13	4	34	25	16	7	37	28	19	10

embracing 5 ring gear teeth is chosen for all the analysis carried out in this work. Figure 4 depicts such a window, which is a rectangular window with cosine tapered ends where the central part is 3 teeth width with an overlap factor of 2 teeth.

Localized faults in planet gear are taken into account in the first test, while a planet bearing fault is considered in the second test. Such two tests are presented and discussed in the following subsections.

#### 4.1. Gear analysis

Two localised tooth faults were artificially introduced on one planet gear of the gearbox first stage. Figure 5 depicts the two faults, namely LFP1 and LFP2. The dimensions of the faults related to axial length of the tooth are 14% and 45% respectively for LFP1 and LFP2. In particular, LFP1 is a small tooth fault introduced on the tooth flank with an electric pen drive. The LFP2 fault, which is introduced via a drilling process, embraces approximately half of the tooth flank.

During tests, the vibration signals were acquired by means of a piezoelectric accelerometer (frequency range 1 to 12000Hz) mounted in radial direction on the gearbox case near the ring gear. A one pulse per revolution optical tachometer is mounted on the gearbox output shaft (planet carrier). Signals were acquired for an extent of 60s with a sample frequency of 204.8kHz. This high sample frequency guarantees to properly acquire the tachometer signal. Vibration signals were subsequently downsampled at 5.12kHz during

287 post processing, in order to embrace the first five meshing components. Tests  
288 were performed at different conditions of driving speed and applied torque.  
289 The results presented in this work are relative to a nominal driving motor  
290 speed of 20Hz and nominal output shaft torque of 12Nm.

291 Figure 6 depicts the time signals captured from the accelerometer for both  
292 sound and faulty conditions. The vibration amplitude related to the two fault  
293 conditions is not increased compared to the sound one. In particular, the  
294 modulation effect due to the planet gear passage toward the accelerometer is  
295 not visible.

296 Diagnostics informations about the faulted planet gear can be obtained  
297 by extracting the signals of each planet gear from the global vibration sig-  
298 nal captured by the accelerometer. In order to do that the TSA technique  
299 proposed by McFadden [10] can be used. The application of this technique  
300 relies on the knowledge of the position of the planet gears with respect to  
301 the accelerometer. This position can be determined from the ring gear TSA  
302 by identifying the locations of the maximum vibration amplitude. Figure 7  
303 depicts the ring gear TSA for both sound and faulted conditions. The three  
304 ring gear TSAs are essentially the same, sure enough these represent the ring  
305 gear signal which does not change from the sound to the faulty gearbox con-  
306 ditions. The relative position of each of the planet gears with respect to the  
307 transducer is not visible. Because of the geometrical and material properties  
308 of the gearbox under test, the transfer function between the transducer and  
309 the planet gear (Figure 1 (b)) is flat for the most part. This is mainly due  
310 to the mass, damping and stiffness properties of the gearbox. In this case  
311 the position of the planet gears is not detectable with the amplitude demod-  
312 ulation techniques, leading to a poor evaluation of the planet gear TSAs.  
313 In particular, Figure 8 depicts the results of the amplitude demodulation  
314 [15], where a filter bandwidth of 18 orders around the first (Figure 8(a)),  
315 second (Figure 8(b)), third (Figure 8(c)) and fourth (Figure 8(d)) meshing  
316 component is used in order to extract the amplitude modulation from the  
317 sound ring gear TSA. As stated before, no interesting information about the  
318 position of the planet gears can be obtained with this analysis due to the  
319 flatness of the transfer function  $h(t)$ .

320 Figure 9 depicts the core of this work. In particular, Figure 9 shows  
321 the results of the application of the two proposed methods on the ring gear  
322 TSA for both the LFP1 and LFP2 fault conditions, respectively. The two  
323 methods, the first one based on the  $P_x$  and the second one based on the  
324  $MCF$ , give very close results, i.e. the points related to the maxima and

325 minima of the two functions are almost the same. Small differences of 1-2  
326 teeth proved to not change the output results, and for that reason only the  
327  $P_x$ -method results will be shown in the figures later on.

328 In particular, it is possible to see that for the case of the LFP1 fault  
329 (Figure 9 (b) and (c)) the first maximum is reached around ring gear tooth  
330 8. This means that the starting position of one planet gear, which could be  
331 the planet gear 1 without loss of generality, is shifted of an angle covered by  
332 8 ring gear teeth with respect to the transducer. By inspecting the other two  
333 maxima of the functions, or via geometric considerations, one can conclude  
334 that the other two planet gears are shifted by an amount of 44 and 80 ring  
335 gear teeth with respect to the transducer (Figure 9 (b) and (c)). Analogous  
336 considerations can be performed for the LFP2 fault. Specifically, the first  
337 maximum is reached around the same ring gear tooth 8, which means that  
338 one planet gear is shifted of an angle covered by 8 ring gear teeth with  
339 respect to the transducer (Figure 9 (e) and (f)). The other two planet gears  
340 are shifted of 44 and 80 ring gear teeth, respectively.

341 In order to assess the validity of the proposed methodology, the vibration  
342 signal of the planet gears are extracted with an increasing shift from 1 to  
343 108 ring gear tooth. Therefore, 108 planet gear TSAs are obtained, the  
344 Peak Hold of these TSAs (i.e. the maximum amplitude value of each TSA)  
345 is taken into account and compared with the results of  $P_x$  and  $MCF$  in  
346 Figure 9. It is possible to see a good match between the maximum values in  
347 the  $P_x$  and  $MCF$  functions with respect to the Peak Hold of the planet gear  
348 vibrations. In particular, for the LFP2 fault (Figure 9 (d)) it is possible to  
349 see an increasing in the amplitude content on a range of 30 ring gear teeth  
350 under the transducer, while for the LFP1 fault a small portion of about  
351 5 ring gear teeth is affected by a small amplitude increase. This position  
352 information can be used in order to extract the vibration signal of the planet  
353 gears with the TSA technique proposed by McFadden. Figure 10 depicts the  
354 result of this operation for the LFP1 fault case, where the starting position  
355 of the averaging process is obtained by shifting the vibration signal of an  
356 angle covered by 8 ring gear teeth (first maximum in the  $P_x$  function). The  
357 averaging process can extract the vibration signal related with each planet  
358 gear in a precise manner. As depicted in Figure 10 (a) a small variation of  
359 the vibration amplitude can be seen in the planet gear 1 TSA. This small  
360 amplitude variation is not suitable for a sure fault detection and further  
361 analyses are needed. In particular, Figure 11 compares the results of the  
362 extraction of the planet gear 1 TSA with three different signal shifts. In

363 Figure 11 (a) the signal is shifted of an angle covered by 8 ring gear teeth,  
364 which is the closest position between transducer and planet gear. In Figures  
365 11 (b-c) the signal is shifted of an angle covered by 35 and 62 ring gear teeth,  
366 respectively.

367 The first shift (i.e 35 teeth) correspond to the midpoint between the  
368 closest and the farthest position of the planet gear 1 with respect to the  
369 transducer, whilst the last shift, which corresponds to a minimum of both  
370  $P_x$  and  $MCF$  functions, is the farthest position of planet gear 1 with respect  
371 to the transducer. As one can see, no evidence of variation in the vibration  
372 amplitude can be detected in Figures 11 (b-c). This result highlights the  
373 importance of the knowledge of the relative position of the planet gear with  
374 respect to the transducer, in particular for function  $h(t)$  particularly flat.  
375 Figure 12 plots the result of the TSA of the planet gears for the LFP2 fault  
376 case. These averages are performed by shifting the signal for an amount  
377 corresponding to the first maximum of the  $P_x$  and  $MCF$  functions (i.e. 8  
378 ring gear teeth). It is possible to see a strong variation in the signal amplitude  
379 of the planet gear 1 TSA (Figure 12 (a)), which corresponds to the artificial  
380 fault LFP2 inserted in the planet gear during test, and in addition, other  
381 two small variations are visible around tooth # 24 and 26. These amplitude  
382 variations are probably related to tooth profile errors which were already  
383 existent in the planet gear before test, due to the manufacturing process.

384 As in the case of LFP1 fault, Figure 13 compares the results of the extrac-  
385 tion of the planet gear 1 TSA with three different signal shifts. The first one  
386 deals with the first maximum of the  $P_x$  and  $MCF$  functions (i.e. 8 ring gear  
387 teeth), which is the closest position between transducer and planet gear; the  
388 second one refers to the midpoint between the closes and the farthest posi-  
389 tion between transducer and planet gear; the third one refers to a minimum  
390 in the two functions which is the farthest position of the planet gear 1 with  
391 respect to the transducer (i.e. 62 ring gear teeth). Comparing Figures 13 (a),  
392 (b) and (c), it is possible to see that when the planet gear is near the trans-  
393 ducer, the engaging of the faulted tooth can be well highlighted, whereas it  
394 could be merely visible leading to a poor fault identification. This result indi-  
395 cates that the proposed methodologies are effective for the evaluation of the  
396 planet gear position with respect to the transducer, leading to the detection  
397 of the faulty planet gear. In particular, if the real position of the planet gear  
398 with respect to the transducer is not correctly determined, the signature of  
399 the faulty planet gear cannot be suitably extracted from the noisy vibration  
400 response.

Table 4: Planet bearing data

Needle number	17
Needle diameter [mm]	2
Mean bearing diameter [mm]	11
Pressure angle [deg]	0

#### 401 4.2. Bearing analysis

402 Planet bearings are full-complement needle bearings without cage. This  
 403 arrangement consists of a collection of rollers arranged loosely between the  
 404 pin, which connects the gear to the carrier, and the bore of the gear. The  
 405 pin and the gear bore act as inner and outer races, respectively (Figure 14  
 406 (a)). A localised fault was artificially introduced on the inner ring of a planet  
 407 bearing (carrier pin) via a drilling process. **The angular length of the fault**  
 408 **is 28deg, the depth is approximately 0.5mm and the axial length is the 65%**  
 409 **of the inner ring width.** Figure 14 shows a full-complement needle bearing  
 410 of the MP105IS2 planetary gearbox as well as the localised fault under test.  
 411 Bearing data are depicted in Table 4.

412 The test set-up is the same presented in Sec. 4.1. The only differences  
 413 are the mounting position of the optical tachometer, which is placed on the  
 414 gearbox input shaft (first stage sun gear), and the downsampling frequency of  
 415 the vibration data that is set at 51.2kHz. The fault on the bearing has been  
 416 tested at two different torque loads only (12 Nm and 0 Nm). The results  
 417 shown hereafter are consequently related to the loaded case.

418 Figure 15 depicts the time signals captured from the accelerometer for  
 419 both sound and faulty conditions. Once again the vibration amplitude re-  
 420 lated to the faulty condition is not increased compared to the sound one. In  
 421 particular, the RMS and Kurtosis values evaluated on the time signals for  
 422 both the two conditions are essentially the same, i.e.  $\text{RMS}_{\text{Sound}} = 2.18\text{g}$  and  
 423  $\text{Kurt}_{\text{Sound}} = 4.7$ ,  $\text{RMS}_{\text{Fault}} = 1.89\text{g}$  and  $\text{Kurt}_{\text{Fault}} = 5.8$ . Only the kurtosis  
 424 value shows a small increment, however this increment does not justify the  
 425 presence of a bearing fault. **Figure 15 could also be compared with Figure 6,**  
 426 **in both cases the diagnostics of faults is almost impossible without a proper**  
 427 **pre-processing of the data.**

428 Figure 16 shows the corresponding spectra. It is possible to see that for  
 429 both conditions the components dominating the spectra are related to the  
 430 meshing frequencies of the two stages. In more detail, the first stage meshing

431 frequency is 432Hz whilst the second stage meshing frequency is 86.4Hz.  
432 Sidebands arise around the two meshing frequencies for both sound and faulty  
433 conditions. It is a matter of fact that in planetary gearbox sidebands are  
434 not related to the presence of a fault but are due to the relative motion of  
435 the planets with respect to the accelerometer which is mounted on the ring  
436 gear. An increase of the amplitude of the sidebands around the first stage  
437 meshing frequency is visible in Figure 16 (b). In particular, these sidebands  
438 are related to the rotation frequency of the first stage carrier. This effect  
439 could be associated to an abnormal rotation of the first stage carrier resulting  
440 from an abnormal gear planet rotation due to the planet bearing fault. In  
441 his well known handbook on gear analysis, Taylor [16] states that when the  
442 amplitude of the sidebands on the low side of gear mesh frequency is higher  
443 than the upper sidebands, looseness is indicated. In Figure 16 (b) the lower  
444 sideband (428 Hz) is quite higher than the gear mesh frequency (432 Hz),  
445 pointing out a looseness condition in the planet gear with the faulted bearing.  
446 Moreover, no evidence of a resonance zone excited by the impulses produced  
447 by the fault is present in the frequency domain between 0 Hz and 25.6 kHz.  
448 These results cannot provide proper diagnostics information and additional  
449 analyses have to be carried out.

450 Figure 17 shows the Cyclic Spectra for both sound and faulty conditions.  
451 It is possible to see that there is a strong release of power at the rotation fre-  
452 quency of the first stage planet carrier (4Hz) and its harmonics. In particular,  
453 for the faulted condition (Figure 17 (b)), there is a strong modulation of the  
454 rotation frequency of the first stage planet carrier by the rotation frequency  
455 of the second stage planet carrier (0.8Hz). This effect could be related to the  
456 floating sun gear arrangement applied in this type of gearbox.

457 It is a matter of fact that in planetary gearbox the radial loads acting  
458 on the sun cancel out, and therefore fixed radial bearings are not necessary  
459 to support the sun gear itself. However, the localised fault in the planet  
460 bearing causes an incorrect engagement between the planet and the sun.  
461 This phenomenon could produce an irregular radial displacement of the sun  
462 gear during its rotation, which manifests itself as a modulation of the sun  
463 rotation frequency. Actually, these results can highlight the malfunctioning  
464 behaviour of the planetary gearbox. However, no diagnostics information  
465 such as the type and the position of the fault can be obtained, in particular,  
466 the cyclic frequency of the inner race fault (111.2725Hz) is not visible inside  
467 the signal Cyclic Spectrum (Figure 17 (b)).

468 Diagnostics information about the faulted planet bearing can be obtained



469 by extracting, from the global vibration signal captured by the accelerom-  
470 eter, the signals of each planet gear. In particular the power flow method  
471 has been used in this paper in order to find the initial angular position of  
472 the planets with respect to the transducer. In order to do that the TSA  
473 technique proposed by McFadden [10] can be used. De facto, the TSA sig-  
474 nal is only the deterministic counterpart of the raw signal, while the bearing  
475 fault information is included in the second order cyclostationary counterpart.  
476 Therefore, the bearing analysis is performed on the extracted planet signal  
477 before averaging. After that, by the evaluation of the Cyclic Power on the  
478 extracted signals it is possible to obtain information on how the power is  
479 released by that particular component, highlighting the presence of a fault in  
480 a particular planet bearing. The extracted planet signals are in the angular  
481 domain, thus the corresponding Cyclic Powers belongs to the the cyclic order  
482 domain. The link between cyclic orders and cyclic frequencies is the rotation  
483 frequency of the extracted component, i.e. sun gear or planet gear. In this  
484 case one has to take into account the Willis formula. If  $f_p$  is the rotation  
485 frequency of the planet gear and  $f_c$  is the rotation frequency of the planet  
486 carrier, then the relation between cyclic frequency and cyclic order for the  
487 planet gear is  $|f_p - f_c| = 11.0769\text{Hz}$ .

488 Figure 18 shows the Cyclic Power evaluated on the extracted planet sig-  
489 nals in both sound and faulty conditions in the cyclic order range  $0 \div 12$ . In  
490 the Cyclic Power of the sound planet (Figure 18(a)), three distinct compo-  
491 nents are visible. The first one (0.36O) is related to the rotation of the first  
492 stage planet carrier, whilst the others (2O and 6O) are linked to the planet  
493 rotation frequency. On the contrary, Figure 18(b) shows the presence of two  
494 distinct cyclic orders, the first one (2O) is related to the planet rotation fre-  
495 quency, while the second one (9.6O) is the inner race fault order of the planet  
496 bearing. By comparing Figures 17 (b) and 18(b) it is possible to see that,  
497 in order to diagnose a fault inside a planet bearing, the planet signal must  
498 be extracted from the main vibration signal. Sure enough, the cyclic fault  
499 frequency is not visible in the Cyclic Spectrum of the main vibration signal  
500 (Figure 17 (b)), but only in the Cyclic Spectrum of the planet gear signal  
501 (Figure 18(b)).

502 It must be pointed out the importance of the pre-processing performed on  
503 the basis of tooth mesh period in the bearing analysis. Usually the bearing  
504 fault frequencies and the gear frequencies cover different ranges of the spec-  
505 trum, how can the proposed method be able to retrieve bearing information  
506 under these circumstances? It is a matter of fact that the cause of the vibra-

507 tion signal, i.e. the fault on the bearing, is strictly related to two elements:  
508 the geometry of system, and the kinematics of the system. It is well known  
509 there is a direct proportionality between the fault frequency, the geometry  
510 of the bearing and the rotational frequency of moving ring (kinematics). In  
511 common applications both the geometry and kinematics are given, as in an  
512 asynchronous motor working at constant speed. In other applications like  
513 the planetary gearbox, the bearing could be placed on subsystems (i.e. the  
514 carrier) whose kinematics depends on other mechanisms kinematics (the sun  
515 and the ring gears). Moreover, the relative position between the source of  
516 the vibration (i.e. the bearing) and the sink (i.e. the sensor) changes cycli-  
517 cally. A simple, although direct, analysis of the raw data will comprise these  
518 non-trivial aspects. The extraction of the signal of the signal on the basis of  
519 the tooth mesh period allows rebuilding a new vibration data on the basis  
520 of both geometry and kinematics of the gearbox. Please note the fundamen-  
521 tal difference between the gear and bearing diagnostics: both start from the  
522 reconstruction of the vibration signal of the planet, but the gear analysis  
523 needs a further processing by means of TSA, while the bearing analysis is  
524 performed on the reconstructed signal directly.

## 525 5. Concluding Remarks

526 In this paper a comprehensive diagnostics of the two main components  
527 of a gearbox is presented. In the available literature papers focus on gears  
528 and bearings separately, leaving a sensible gap anytime the whole gearbox  
529 needs to be monitored. In particular, this paper addresses the diagnostics of  
530 epicyclic gearboxes, which are more complex than ordinary ones. In fact the  
531 relative angular position among an external accelerometer, the planet and  
532 sun gears is cyclic, and a vibration signal of a faulted tooth planet could  
533 be dominated by the vibration of another planet closer to the sensor. Two  
534 procedures for the precise evaluation of the planet gear position have been  
535 presented. The first one is based on the study of the power flows inside the  
536 ring gear TSA, whilst the second method is based on a modified statistical  
537 parameter such as the Crest Factor (*MCF*). The effectiveness of the two  
538 methods are compared on the basis of real data.

539 In the first method the position of the planet gears with respect to the  
540 transducer is obtained by reconstructing the power flow at the cyclic fre-  
541 quency corresponding to the number of planet gears of the planetary gear-  
542 box under test. The second method relies on a modified version of the Crest

543 Factor ( $MCF$ ). In particular, the  $MCF$  is evaluated on a tooth-wide sig-  
544 nal portion, thus obtaining a function and not a single value. The planet  
545 gear position is determined by filtering the so obtained  $MCF$  around the  
546 frequency related to the number of planet gears.

547 The two proposed methods give the same results, highlighting the position  
548 of the planet gears. As these positions are completely determined by the  
549 maxima of the two functions, the entire procedure could be easily automated.

550 From the present analysis it could be concluded that the evaluation of the  
551 relative position between planet gears and transducer is a [useful information](#)  
552 for the effectiveness of the averaging procedure, in particular for flat shaped  
553 transfer function of the gearbox. Actually, if the correct position of the planet  
554 gear with respect to the transducer is not correctly determined, the signature  
555 of the faulty planet gear cannot be extracted from noisy vibration responses.

556 The same procedure allows to deduce further informations on planet bear-  
557 ings health condition. Planet bearings are full-complement needle bearings  
558 without cage. This arrangement consists of a collection of rollers arranged  
559 loosely between the pin, which connects the gear to the carrier, and the bore  
560 of the gear. A localised fault was artificially introduced on the inner ring of  
561 a planet bearing (carrier's pin) via a drilling process in order to prove the  
562 effectiveness of the procedure.

563 In particular the evaluation of the Cyclic Power on the rebuilt signal al-  
564 lows to obtain information on how the power is released. The results indicate  
565 that the proposed methodology can identify the faulted bearing signature.

## 566 6. Acknowledgement

567 This work has been developed within the Advanced Mechanics Labora-  
568 tory (MechLav) of Ferrara Technopole, realized through the contribution of  
569 Regione Emilia-Romagna - Assessorato Attività Produttive, Sviluppo Eco-  
570 nomico, Piano telematico - POR-FESR 2007-2013, Attività I.1.1

## 571 7. References

- 572 [1] Antoni, J., Bonnardot, F., Raad, A., El Badaoui, M.: Cyclostationary  
573 modelling of rotating machine vibration signals. *Mechanical Systems  
574 and Signal Processing* 18, 1285-1314 (2004)
- 575 [2] Gardner, W.A.: The spectral correlation theory of cyclostationary time-  
576 series. *Signal Processing* 11(1), 13-36 (1986)

- 577 [3] McCormick, A.C., Nandi, A.K.: Cyclostationary in rotating machine vi-  
578 brations. *Mechanical Systems and Signal Processing* 12, 225-242 (1998)
- 579 [4] Randall, R.B., Antoni, J.: Rolling element bearing diagnosticsA tuto-  
580 rial. *Mechanical Systems and Signal Processing* 25, 485-520 (2011)
- 581 [5] Antoni, J.: Cyclic spectral analysis of rolling-element bearing signals:  
582 Facts and fictions. *Journal of Sound and Vibration* 304, 497-529 (2007)
- 583 [6] Antoni, J.: Cyclostationarity by examples. *Mechanical Systems and Sig-  
584 nal Processing* 23, 987-1036 (2009)
- 585 [7] S. Braun, *The extraction of periodic waveform by time domain averaging*,  
586 *Acustica*, Vol. 32, No. 2, 1975, pp. 69-77.
- 587 [8] P. D. McFadden, *Interpolation techniques for time domain averaging of  
588 gear vibration*, *Mechanical Systems and Signal Processing*, Vol. 3, No.  
589 1, January 1989, pp. 87-97.
- 590 [9] S. Braun, *The synchronous (time domain) average revisited*, *Mechanical  
591 Systems and Signal Processing*, Vol. 25, No. 4, May 2011, pp. 1087-1102.
- 592 [10] P. D. McFadden, *A technique for calculating the time domain averages of  
593 the vibration of the individual planet gears and sun gear in an epicyclic  
594 gearbox*, *Journal of Sound and Vibration*, Vol. 144, No. 1, 1991, pp.  
595 163-172.
- 596 [11] D. Forrester, *A method for the separation of epicyclic planet gear vi-  
597 bration signatures*, *Acoustical and Vibratory Surveillance Methods and  
598 Diagnostic Techniques*, Senlis, France, October 1998
- 599 [12] P.D. Samuel and D.J. Pines, *Vibration separation and diagnostics of  
600 planetary geartrains*, American Helicopter Society 56th Annual Forum,  
601 Virgian Beach, Va, May 2000.
- 602 [13] P.D. McFadden, *Window Functions for the Calculation of the Time Do-  
603 main Averages of the Vibration of the Individual Planet Gears and Sun  
604 Gear in an Epicyclic Gearbox*, *Journal of Vibration and Acoustics*, Vol.  
605 116, 1994, pp. 179-187.

- 606 [14] P.D. McFadden and J.D. Smith, *An explanation for the asymmetry of*  
607 *the modulation sidebands about the tooth meshing frequency in epicyclic*  
608 *gear vibration*, Journal of Mechanical Engineering Science, Vol. 199, No.  
609 C1, 1985, pp. 65-70.
- 610 [15] P. D. McFadden, *Detecting Fatigue Cracks in Gears by Amplitude and*  
611 *Phase Demodulation of the Meshing Vibration*, Journal of Vibration,  
612 Acoustics, Stress and Reliability in Design, Vol. 108, 1986, pp. 165-170
- 613 [16] J.I. Taylor, *The Gear Analysis Handbook*, Tampa (FL), USA, Vibration  
614 Consultants Inc., 2000.

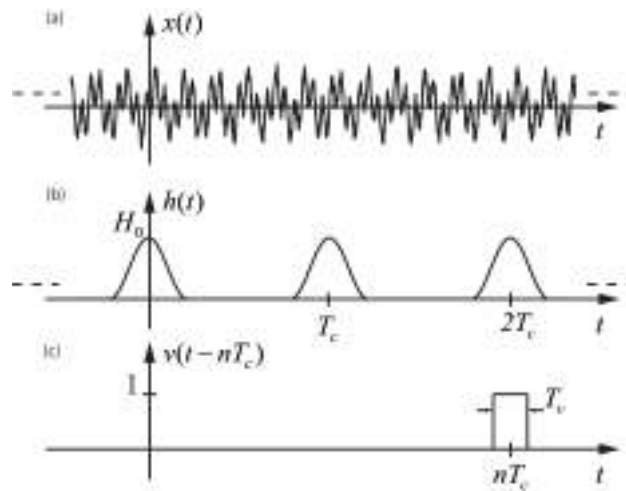


Figure 1: Planet vibration signal measured by a fixed transducer [10]: (a) Time planet vibration signal, (b) Transfer function between planet and transducer (c) windowing function  $v(t - nT_c)$ , where  $n$  is an integer number

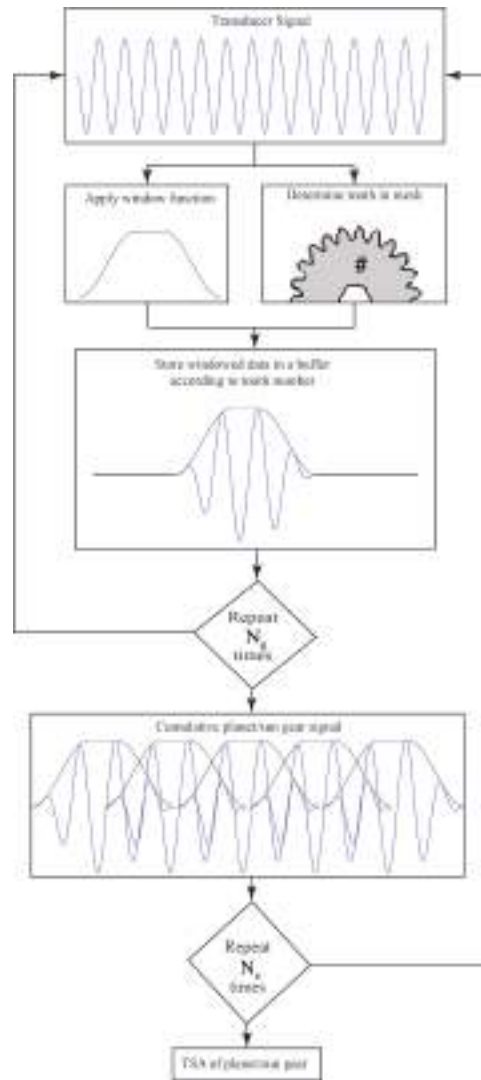


Figure 2: TSA block diagram for planet/sun gear.  $N_g$  is the tooth number of the gear of interest.  $N_e$  is the number of averages.

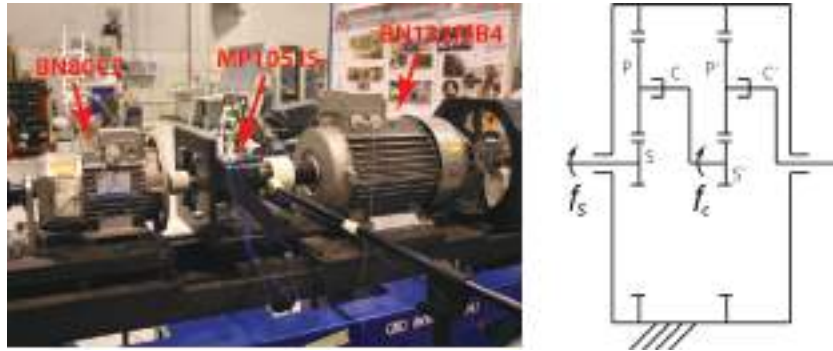


Figure 3: Test-rig

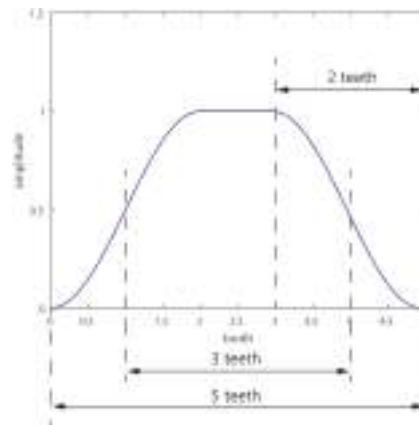


Figure 4: Window function used in the TSA algorithm

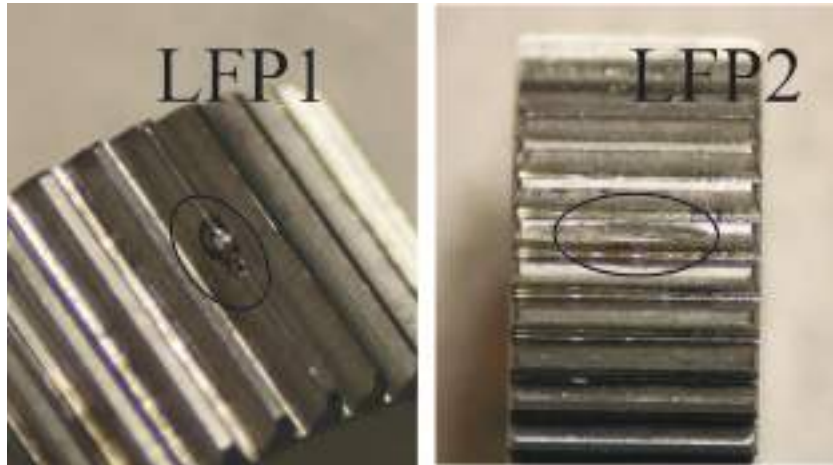


Figure 5: Localised tooth faults

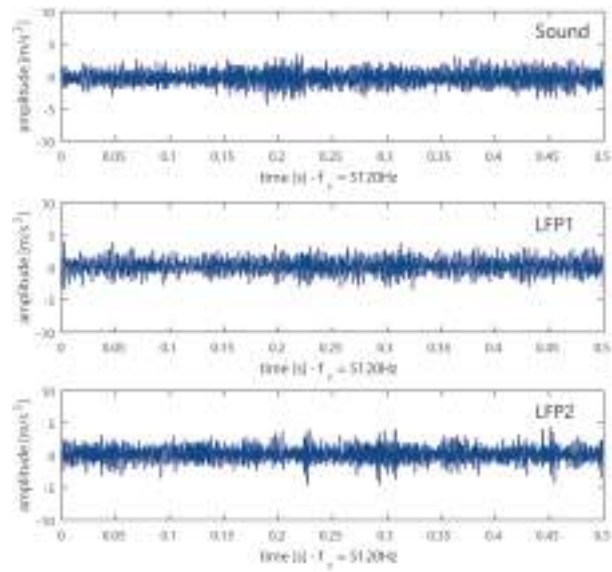


Figure 6: Time signal for two revolutions of the planet carrier: Sound, LFP1 fault, LFP2 fault



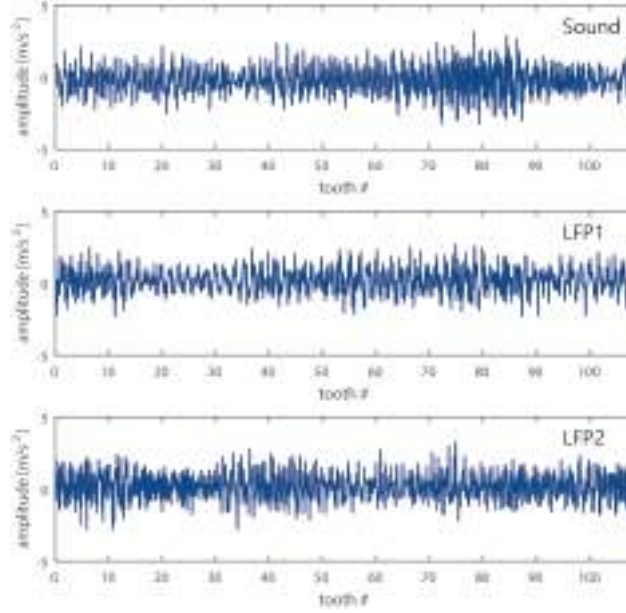


Figure 7: Ring gear TSA (246 averages): Sound, LFP1 fault, LFP2 fault

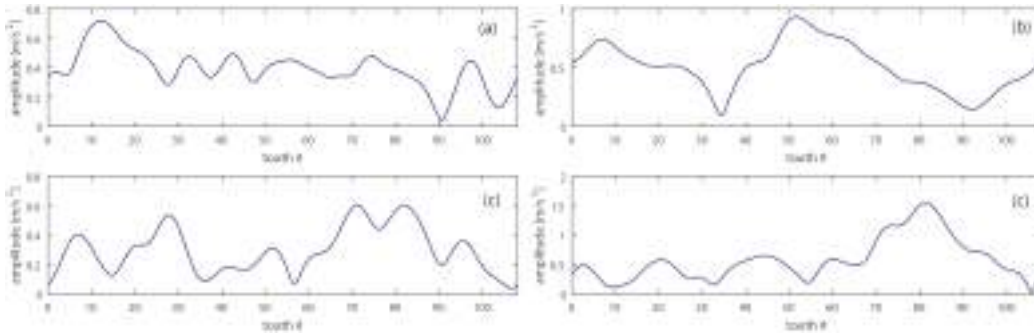


Figure 8: Amplitude modulation of sound ring gear TSA: (a) filtered around the first meshing component, (b) filtered around the second meshing component, (c) filtered around the third meshing component, (d) filtered around the fourth meshing component

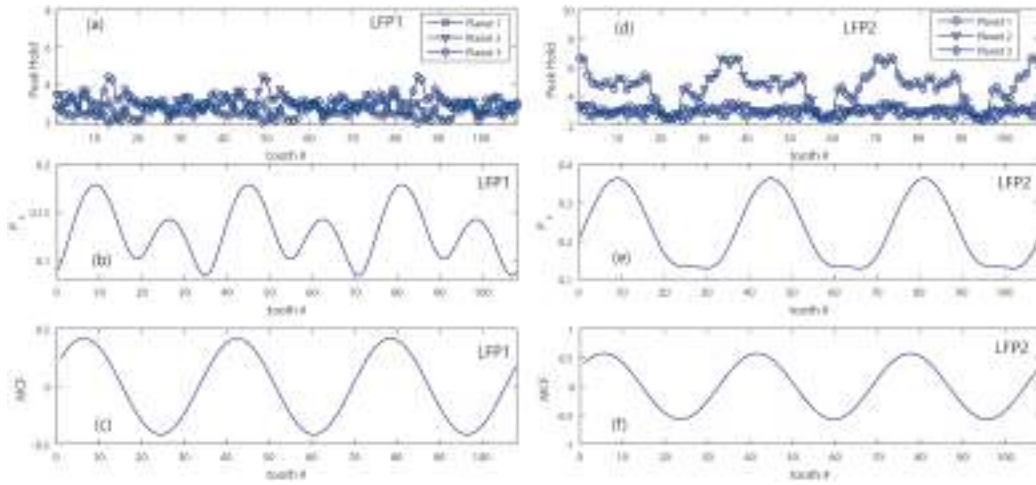


Figure 9: (a) Peak Hold of the planet gear vibrations extracted with an increasing shift from 1 to 108 ring gear tooth for the LFP1 fault, (b)  $P_x$  function for the LFP1 fault, (c)  $MCF$  function for the LFP1 fault, (d) Peak Hold of the planet gear vibrations extracted with an increasing shift from 1 to 108 ring gear tooth for the LFP2 fault, (e)  $P_x$  function for the LFP2 fault, (f)  $MCF$  function for the LFP2 fault

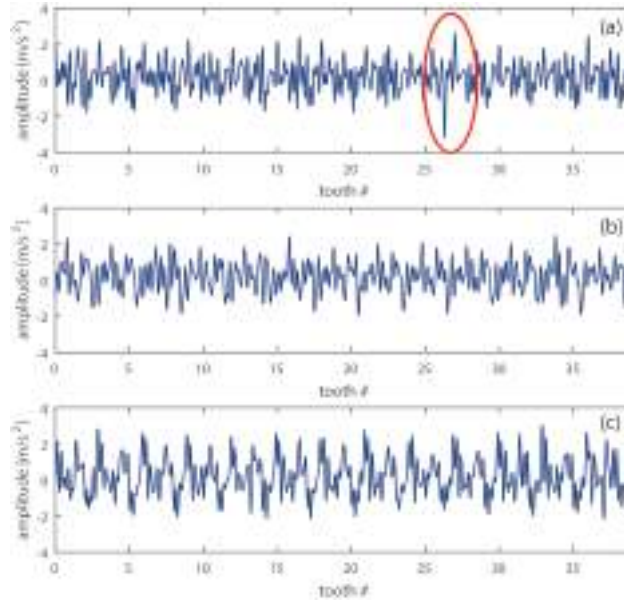


Figure 10: TSA of planet gears for LFP1 fault with an initial phase shift of 8 teeth (18 averages): (a) Planet gear 1, (b) Planet gear 2, (c) Planet gear 3

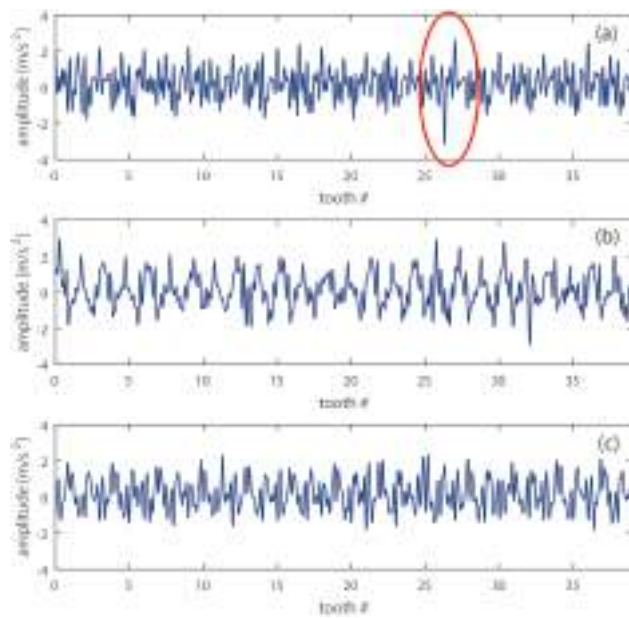


Figure 11: TSA of planet gear 1 for LFP1 fault (18 averages): (a) initial phase shift of 8 teeth, (b) initial phase shift of 35 teeth, (c) initial phase shift of 62 teeth

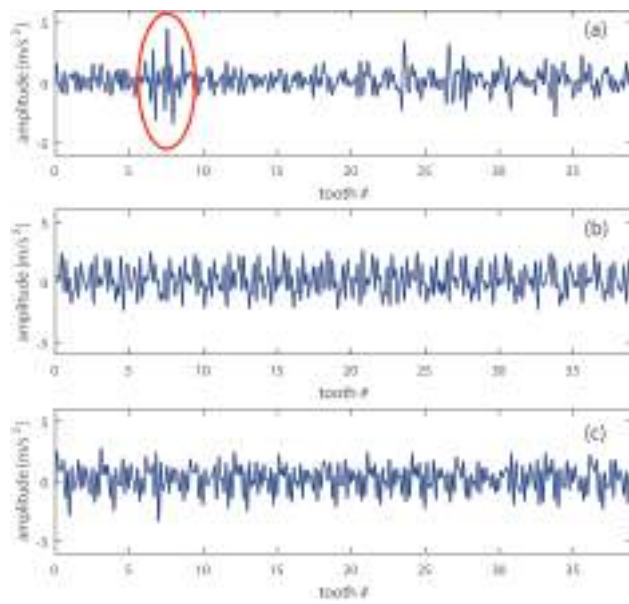


Figure 12: TSA of planet gears for LFP2 fault with an initial phase shift of 8 teeth (18 averages): (a) Planet gear 1, (b) Planet gear 2, (c) Planet gear 3

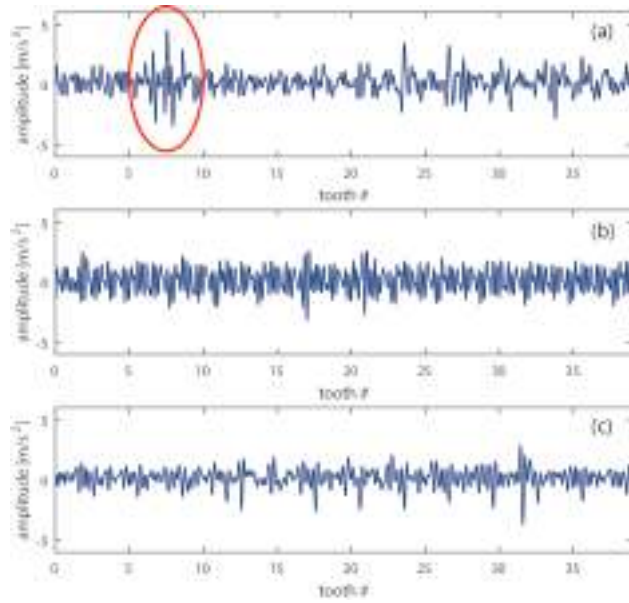


Figure 13: TSA of planet gear 1 for LFP2 fault (18 averages): (a) initial phase shift of 8 teeth, (b) initial phase shift of 35 teeth, (c) initial phase shift of 62 teeth



Figure 14: (a) planet gear full-complement needle bearing, (b) localised fault on the inner race (cage pin) of a planet bearing

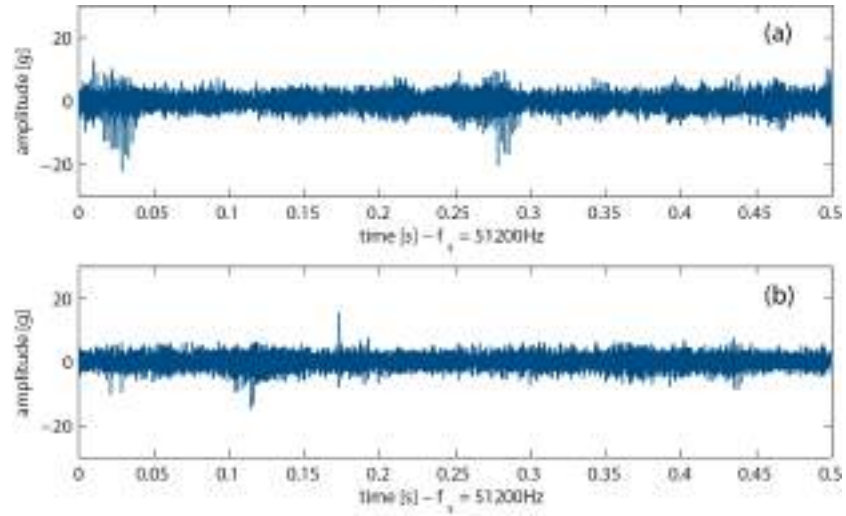


Figure 15: Time signal for 2 revolutions of the planet carrier: (a) Sound, (b) Faulty

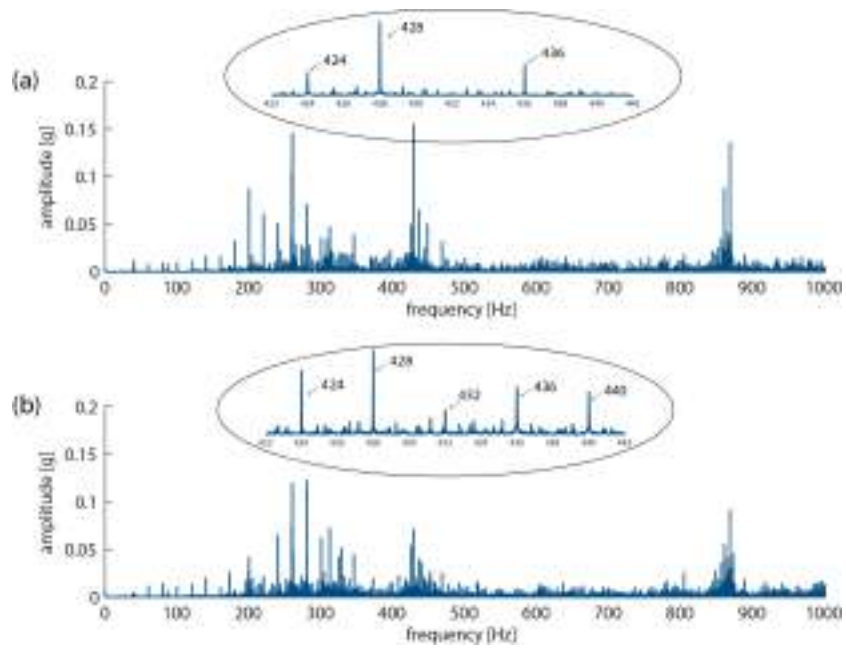


Figure 16: Spectra: (a) Sound, (b) Faulty

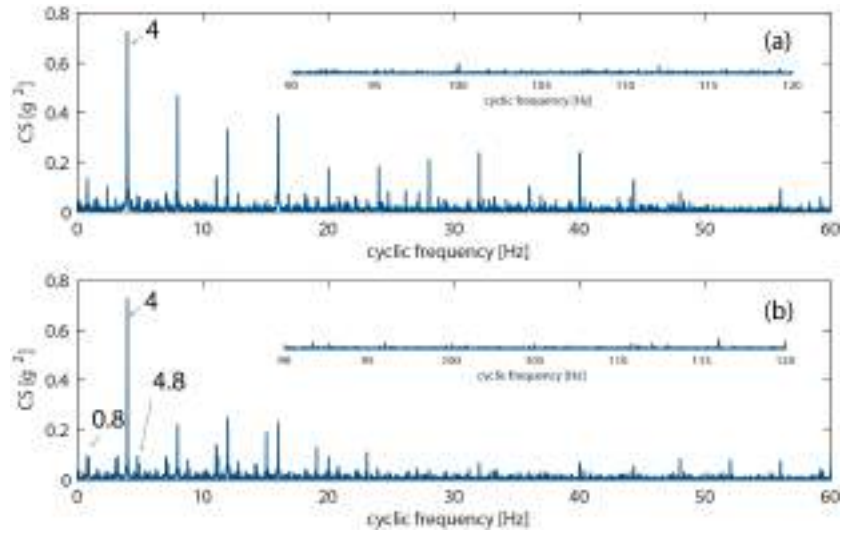


Figure 17: Cyclic Power evaluated on the time signal: (a) Sound, (b) Faulty

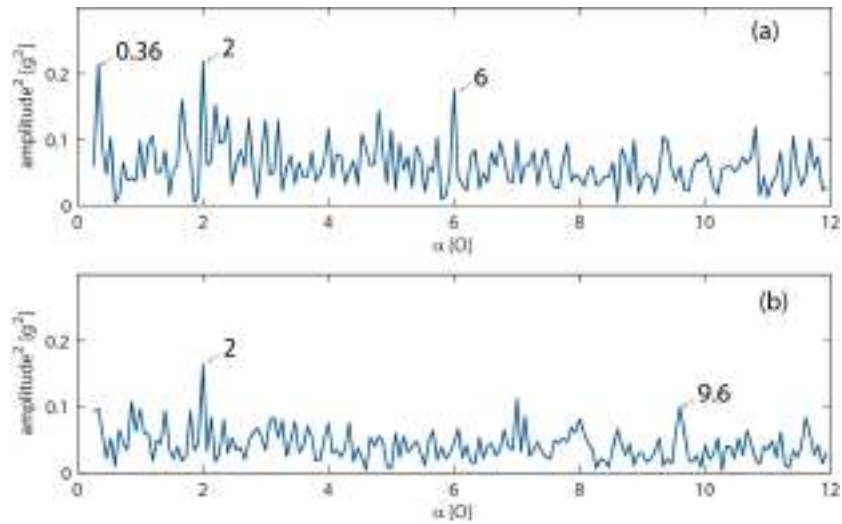


Figure 18: Cyclic Power evaluated on the extracted planet signal: (a) Sound, (b) Faulty